Increasing Fisher Information by Moving-Mesh Reconstruction

Qiaoyin Pan,[1, 2, *] Ue-Li Pen,[2, 3, 4, 5, †] Derek Inman,[2, 6] and Hao-Ran Yu[2, 7]

[1]*School of Physics, Nankai University, 94 Weijin Rd, Nankai, Tianjin, 300071, China*
[2]*Canadian Institute for Theoretical Astrophysics, University of Toronto,*
60 St. George Street, Toronto, Ontario M5S 3H8, Canada
[3]*Dunlap Institute for Astronomy and Astrophysics,*
University of Toronto, Toronto, ON M5S 3H4, Canada
[4]*Canadian Institute for Advanced Research, Program in Cosmology and Gravitation*
[5]*Perimeter Institute for Theoretical Physics, Waterloo, ON, N2L 2Y5, Canada*
[6]*Department of Physics, University of Toronto, 60 St. George, Toronto, ON M5S 1A7, Canada*
[7]*Kavli Institute for Astronomy and Astrophysics, Peking University, Beijing 100871, China*
(Dated: December 12, 2016)

Reconstruction techniques are commonly used in cosmology to reduce complicated nonlinear behaviours to achieve a more tractable linearized system. We study a new reconstruction technique, which uses the Moving-Mesh algorithm to estimate the displacement field from nonlinear matter distribution. We show the performance of this new technique by quantifying its ability to reconstruct linear modes. We study the cumulative Fisher information $I(< k)$ in the matter power spectrum in 130 N-body simulations before and after reconstruction, and find that the linear scale is pushed to $k \simeq 0.3$ h/Mpc after reconstruction. We furthermore find that the non-linear plateau of $I(< k_n)$ is increased by a factor of ~ 50 after reconstruction, from $I \simeq 2.5 \times 10^{-5}/(\text{Mpc}/h)^3$ to $I \simeq 1.3 \times 10^{-3}/(\text{Mpc}/h)^3$ at $k \simeq 2.7$ h/Mpc. This result includes the decorrelation between initial and final fields, which has been neglected in some previous studies, artificially improving their performance. We expect this technique to be beneficial to problems such as baryonic acoustic oscillations and cosmic neutrinos that rely on an accurate disentangling of nonlinear evolution from underlying linear effects.

PACS numbers:

I. INTRODUCTION

Two-point statistics provide complete descriptions of Gaussian density fields and can be computed efficiently even for large data sets. However, nonlinear gravitational evolution leads to highly non-Gaussian matter distributions which require higher order statistics to fully characterize. Such statistics are computationally expensive and can be challenging to map to cosmological parameters. To mitigate these difficulties, it is common to transform the matter field in a way that hopefully reduces non-Gaussianity. For example, Gaussianization transforms have been used to make the logarithmic distribution more Gaussian [1, 2] and wavelet nonlinear Wiener filters have been used to separate Gaussian and non-Gaussian components of the density field [3–5]. *Reconstruction* techniques [6] provide a more effective way by converting matter distributions back to an earlier stage [5].

The quality of these techniques can be quantified by computing the Fisher information [7] present in the power spectrum before and after reconstruction/Gaussianization. Rimes and Hamilton [7] were the first to study the Fisher information in the nonlinear matter power spectrum calculated from N-body simulations. They found that the cumulative information has a plateau on translinear scales ($k \simeq 0.2 - 0.8$ h/Mpc) due to strong coupling between Fourier modes. Qualitatively, this means that the power spectra on these scales give little additional information. Harnois-Déraps et al. [5] computed the cumulative Fisher information for various Gaussianization methods and their combinations and found that while mode coupling is reduced, there is not necessarily an improvement in the cross correlation between the initial density fields and the final nonlinear ones.

In studies of Baryon Acoustic Oscillations (BAO), density fields are subjected to reconstruction which partially inverts nonlinear evolution by applying the negative Zel'Dovich displacement field [8]. The linear density field is typically estimated via Lagrangian perturbation theory (LPT) using the linear Zel'Dovich displacement $-\nabla_q \cdot \boldsymbol{\Psi}(\boldsymbol{q})$ with respect to initial coordiantes $\boldsymbol{q}$ [9]. Yu et al. [10] studied the curl-free, or E-mode, component of the exact displacement field in Lagrangian space and found that the linear density field can be well recovered by this E-mode displacement field. This E-mode reconstruction therefore provides a theoretical target for other reconstruction techniques to be compared with. Recently Zhu et al. [11] described a new reconstruction technique using the Moving-Mesh algorithm (MM), first described in [12, 13], to effectively estimate $\boldsymbol{\Psi}(\boldsymbol{q})$ from only nonlinear density fields. They further showed that even though shell-crossing and vorticity are not recovered, linear density modes are still recovered up to scales relevent to the BAO.

In this paper, we compute the Fisher information recovered after using this new reconstruction scheme on 130 independent N-body simulations, and compared with other methods and unreconstructed fields. The paper

*Electronic address: panda@mail.nankai.edu.cn
†Electronic address: pen@cita.utoronto.ca

is organized as follows. In §II, we briefly describe the computation of the displacement potential using MM algorithm. In §III, we describe the simulations, implementation of the reconstruction and compare the power spectra and cross correlations before and after reconstruction. In §IV, we further compute the correlation matrix and Fisher information before and after reconstruction. Finally, in §V, we summarize our results and discuss the effectiveness of the reconstruction and its potential applications.

II.   RECONSTRUCTION TECHNIQUE

Here we briefly review the MM algorithm used in the new reconstruction technique; for a more complete description we refer the reader to [14]. The aim of the MM algorithm is to estimate the displacement field of mass elements in Lagrangian coordinates from their final Eulerian position only, and from this estimated displacement field one directly reconstructs the linear density field. The general principle is to relate the Eulerian coordinates of a mass element, x^i to a curvilinear system, ξ^μ, such that the mass per grid cell is approximately constant

$$\rho\sqrt{g} = \text{Const.}, \tag{1}$$

where $\sqrt{g} \equiv \det\left|e^i_\mu\right|$ is the volume element of the coordinate transformation matrix $e^i_\mu = \partial x^i/\partial \xi^\mu$. These coordinates are related via a *deformation* field, which we assume to be a pure gradient:

$$x^i = \xi^\mu \delta^i_\mu + \frac{\partial \phi}{\partial \xi^\mu}\delta^{i\mu}, \tag{2}$$

and ϕ is called the *deformation potential* which is chosen to adapt Eq. 1. Numerically, we iteratively solve for the deformation potential via a diffusion equation,

$$\partial_\mu(\rho\sqrt{g}e^\mu_i\delta^{i\nu}\partial_\nu\dot{\phi}) = \Delta\rho, \tag{3}$$

where $\Delta\rho = \bar{\rho} - \rho\sqrt{g}$ is the difference in density due to displacing the grids. A detailed description of the analytical formulation can be found in the adaptive particle mesh and moving mesh (MM) hydrodynamics algorithms [12, 13]. Eq. 3 can be solved by multi-grid algorithm[12–14]. Then the estimated displacement field is given by

$$\tilde{\boldsymbol{\Psi}}(\boldsymbol{\xi}) = \nabla\phi(\boldsymbol{\xi}), \tag{4}$$

and the reconstructed density field is given by

$$\delta_R(\boldsymbol{\xi}) = -\nabla \cdot \tilde{\boldsymbol{\Psi}}(\boldsymbol{\xi}) = -\nabla^2\phi(\boldsymbol{\xi}). \tag{5}$$

III.   IMPLEMENTATION AND POWER SPECTRA

We use CUBEP^{3}M [15] to run 140 simulations with a box size of 600 Mpc/h and 512^3 particles. For these simulations, we use cosmological parameters $\Omega_m = 0.321$, $\Omega_\Lambda = 1 - \Omega_m = 0.679$, $h = 0.67$, $\sigma_8 = 0.83$, and $n_s = 0.96$. The initial conditions are computed by transfer function [16] at $z = 100$. Zel'dovich approximation is used to calculate the displacement and initial velocities of particles.

We use the Voronoi tessellation method [17] to estimate the density contrast $\delta_N = \rho/\langle\rho\rangle - 1$ (N stands for nonlinear density from simulation) from particle distributions, and apply the MM reconstruction to these fields with 512^3 grids. The reconstruction code solves the displacement potentials iteratively until the root mean square (rms) of the results drop from ~ 7.5 to 0.20. For different simulation samples, a different number of iterations are required to get the results of the same rms. A total of 130 simulations converged to the target rms within 2000 iterations, and we use these results for the calculation in this paper. A 2-D projection of one layer of the deformed mesh and the original density field on the mesh are shown in Fig. 1. As expected, the deformed mesh traces the structure very well and the deformed grids do not cross each other, even in the 2-D projection.

We study the Fisher information in the matter power spectra. More generally, the cross power spectrum $P_{\alpha\beta}(k)$ for species α and β ($\alpha = \beta$ for auto power spectrum) is defined as

$$\langle\delta^\dagger_\alpha(\boldsymbol{k})\delta_\beta(\boldsymbol{k'})\rangle = (2\pi)^3 P_{\alpha\beta}(k)\delta_{3\text{D}}(\boldsymbol{k} - \boldsymbol{k'}), \tag{6}$$

where δ_α and δ_β are any two fields and $\delta_{3\text{D}}$ is the three-dimensional Dirac delta function. We typically consider instead the dimensionless power spectrum, $\Delta^2_{\alpha\beta}(k)$, defined as

$$\Delta^2_{\alpha\beta}(k) \equiv \frac{k^3 P_{\alpha\beta}(k)}{2\pi^2}. \tag{7}$$

In the left panel of Fig. 2, we show the matter auto power spectrum of linear theory density fields δ_L, nonlinear density fields (δ_N) from simulations and reconstructed density fields ($\delta_R = -\nabla^2\phi$). For the simulation results, we use the average value of all 130 simulations and show 1σ standard deviations as error bars.

To quantify the cross-correlation between fields, we compute the cross correlation coefficient $r_{\alpha\beta}(k) \equiv P_{\alpha\beta}/\sqrt{P_{\alpha\alpha}P_{\beta\beta}}$. In the right panel of Fig. 2, we show r_{NL} and r_{RL}. We see that, compared with δ_N, δ_R is much better correlated with δ_L. We compare our reconstruction correlation coefficient to that of the E-mode reconstruction, r_{EL}, ($\delta_E(\boldsymbol{q}) = -\nabla_q \cdot \boldsymbol{\Psi}(\boldsymbol{q})$) computed in Yu et al. [10]. Even though r_{RL} decreases from r_{EL} in the non-linear regime, due to the fact that the MM reconstruction cannot recover the shell-crossing present on these scales, we find that linear modes are recovered successfully on scales $k \simeq 0.05 - 0.3$ h/Mpc. Specifically, the scale where $r(k) = 1/2$ increases from $k \simeq 0.2$ h/Mpc to 0.8 h/Mpc after reconstruction. In comparison with the results of Zhu et al. [14], we find the correlation coefficient falls off at slightly lower wave numbers, which we attribute to using fewer particles per simulation.
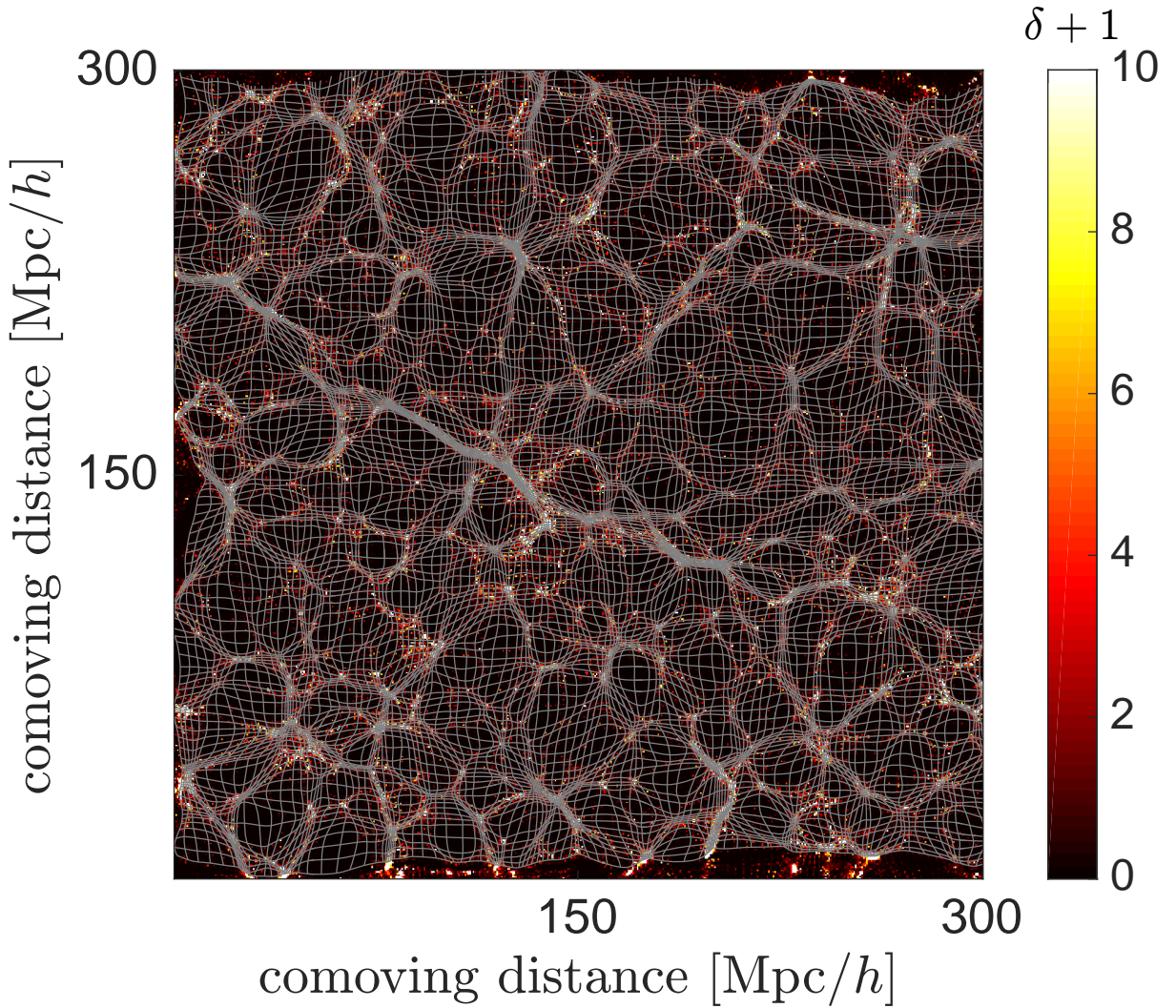
FIG. 1: Illustration of MM reconstruction. The 2-D projection of one layer of the deformed mesh of a sample N-body simulation is shown as curved white lines. The density $\rho/\langle\rho\rangle = 1 + \delta$ on the mesh is shown underneath. For clarity, the scale of the density field is cut to 300 Mpc/h, and only every other grid is plotted.

IV. FISHER INFORMATION CONTENT

Mathamatically, the Fisher information I of the initial scale invariant matter power spectrum, A, is defined as

$$I_A \equiv -\left\langle \frac{\partial^2 \ln\mathcal{L}}{\partial \ln A^2} \right\rangle, \qquad (8)$$

where $\mathcal{L}$ is the likelihood [18]. In this paper, the word "information" and the symbol "I" both implicitly mean cumulative Fisher information of A. For Gaussian fields, the likelihood depends on parameters only through the power spectrum $P(k)$, so I can be written as

$$I = -\left\langle \sum_{k,k'} \frac{\partial \ln P(k)}{\partial \ln A} \frac{\partial^2 \ln\mathcal{L}}{\partial \ln P(k)\partial \ln P(k')} \frac{\partial \ln P(k')}{\partial \ln A} \right\rangle, \quad (9)$$

where the angle bracket averages over realizations [7]. Eq. 9 can be written in a simpler form in two aspects.

Firstly, we simplify the derivative term $\partial \ln P(k)/\partial \ln A$. For a given density field δ_α, we can conveniently decompose it into a correlated, linear component, and a uncorrelated, noise component with respect to δ_L

$$\delta_\alpha(k) = r'(k)\delta_L(k) + \delta_n(k), \qquad (10)$$

where the noise term $\delta_n(k)$ is defined such that the correlation $\langle \delta_L^\dagger(k)\delta_n(k)\rangle = 0$. To solve r', we correlate both sides with δ_L and the uncorrelated noise term drops out,

$$\langle \delta_L^\dagger(k)\delta_\alpha(k)\rangle = r'(k)\langle \delta_L^\dagger(k)\delta_L(k)\rangle, \qquad (11)$$

and by the definitions of cross correlation coefficient $r_{\alpha L}(k) \equiv P_{\alpha L}/\sqrt{P_{\alpha\alpha}P_{LL}}$ and bias $b^2(k) \equiv P_{\alpha\alpha}/P_{LL}$, we can solve for r' as

$$r'(k) = \frac{P_{\alpha L}(k)}{P_{LL}(k)} = r_{\alpha L}(k)b(k). \qquad (12)$$

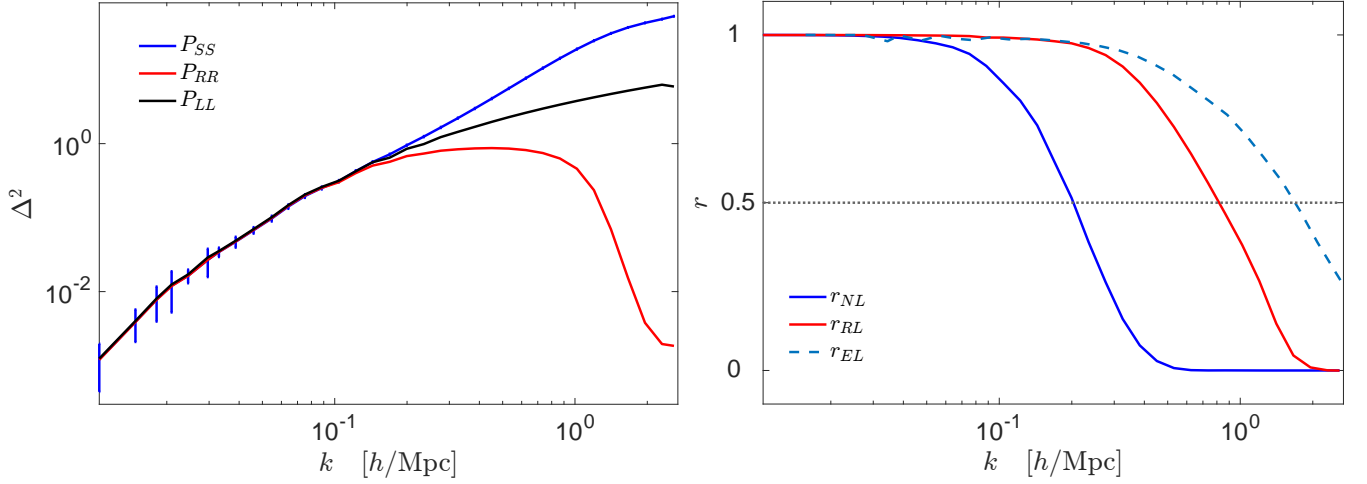To find the nonlinear term, we square both sides of Eq. 10

FIG. 2: *Left.* The dimensionless power spectrum computed via linear theory (black), the mean value of 130 N-body simulations with 1σ error bars (blue), and reconstruction of the simulations (red). *Right.* The cross correlation function between simulation and linear densities r_{NL} (blue), MM reconstructed and linear densities r_{RL} (red), and E-mode reconstruction r_{EL} (dashed blue) from Yu et al. [10].

and the cross term of the right hand side vanishes,

$$\langle \delta_\alpha^\dagger(k)\delta_\alpha(k)\rangle = r_{\alpha L}^2(k)b^2(k)\langle \delta_L^\dagger(k)\delta_L(k)\rangle + \langle \delta_n^\dagger(k)\delta_n(k)\rangle, \tag{13}$$

and find

$$P_{\alpha\alpha}(k) = r_{\alpha L}^2(k)b^2(k)P_{LL}(k) + P_{nn}(k). \tag{14}$$

With the help of Eq. 12 and Eq. 14, we get

$$\frac{\partial \ln P(k)}{\partial \ln A} = r_{\alpha L}^2(k)b^2(k)\frac{P_{LL}(k)}{P_{\alpha\alpha}(k)} = r_{\alpha L}^2(k). \tag{15}$$

Secondly, we simplify $\partial^2 \ln\mathcal{L}/\partial \ln P(k)\partial \ln P(k')$ by using the fact that its expectation value is the Fisher matrix. For Gaussian fields, this is equal to the inverse of the covariance matrix which is diagonal with elements given by the number of modes in each bin (when considering $\boldsymbol{k}$ and $-\boldsymbol{k}$ as the same mode). We can extend this definition to non-Gaussian fields, by taking into account that the covariance matrix is no longer diagonal [7]. Thus, we write the Fisher information in terms of matrix multiplication:

$$I(<k_n) = r^2(k)^{\mathrm{T}}\left[\mathrm{C}_{\mathrm{norm}}^{-1}(k,k')\right]_{<k_n} r^2(k'), \tag{16}$$

where

$$\mathrm{C}_{\mathrm{norm}}(k,k') = \frac{\mathrm{Cov}(k,k')}{\langle P(k)\rangle\langle P(k')\rangle} \tag{17}$$

is the normalized covariance matrix, and r is the mean cross correlation of a given density field with δ_L and the subscript $<k_n$ indicates the matrix is set to zero for modes $k, k' > k_n$. The elements of the covariance matrix are defined as

$$\mathrm{Cov}(k,k') \equiv \frac{\sum_{i,j=1}^{N}\left[P_i(k) - \langle P(k)\rangle\right]\left[P_j(k') - \langle P(k')\rangle\right]}{N-1}, \tag{18}$$

where N is the total number of simulations and angle bracket average these simulations.

The cross-correlation coefficient matrix, or for short the correlation matrix, is defined as

$$\mathrm{Corr}(k,k') = \frac{\mathrm{Cov}(k,k')}{\sqrt{\mathrm{Cov}(k,k)\,\mathrm{Cov}(k',k')}}, \tag{19}$$

representing the correlation between different k modes. The correlation matrices for nonlinear and reconstructed power spectra are shown in the upper-left and lower-right sections of Fig. 3. By definition, the correlation matrix is symmetric with unit diagonal allowing us to overlay the two matrices. For the nonlinear case, it is almost diagonal in the linear regime, $k \lesssim 0.07\ h/$Mpc. The off-diagonal elements are produced by strong mode coupling on nonlinear scales and the super-survey tidal effect which is small on linear scales but dominates in the weakly nonlinear regime [19]. The correlation matrix for the non-linear power spectra has a small amount of negative elements ($\mathrm{Corr} \gtrsim -0.18$), which should vanish with more simulations [20]. For the reconstructed correlation matrix, the linear regime extend up to $k \simeq 0.3\ h/$Mpc. However, the number and magnitude of negative off-diagonal elements also increases ($\mathrm{Corr} \gtrsim -0.49$).

The Fisher information is proportional to the volume. We plot the Fisher information per unit volume of the power spectra of δ_N, δ_L and δ_R in the left panel of Fig. 4. The Fisher information of the linear power spectra is equal to the number of k-modes, N_k. As expected, Fisher information of δ_N drops from δ_L on scale $k \simeq 0.05$ $h/$Mpc, and has a flat plateau in the nonlinear regime, with a saturated value of $I \simeq 2.5 \times 10^{-5}/(\mathrm{Mpc}/h)^3$, indicating the absence of independent information in the nonlinear regime. In comparison, the information curve of δ_R power spectra keeps increasing roughly the same as the linear information until $k \simeq 0.3\ h/$Mpc, and reaches a value of $I \simeq 1.3 \times 10^{-3}/(\mathrm{Mpc}/h)^3$ at $k \simeq 2.7\ h/$Mpc,
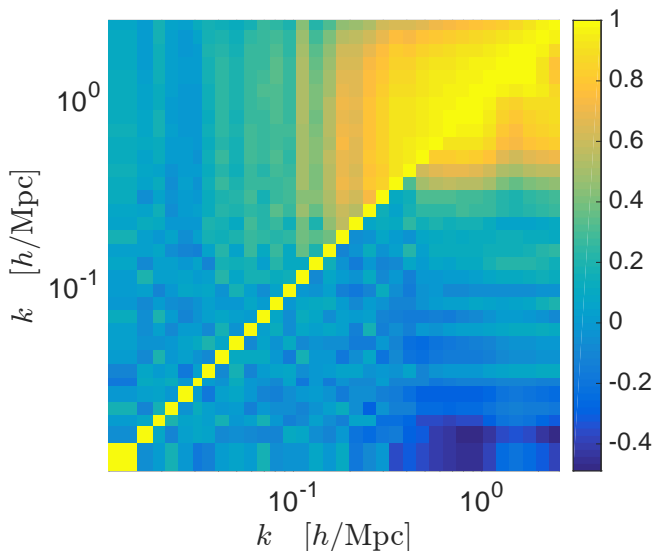
FIG. 3: The correlation matrix from 130 non-linear power spectra (the upper-left elements) and reconstructed power spectra (the lower-right off-diagonal elements).

increased by a factor of 50. We compare the Fisher information given by the MM reconstruction method with the logarithmic density mapping method [2] as an example to illustrate its strength. We find that MM reconstruction gives over 10 times more information than it.

To test the upper limit of information that the MM reconstruction can recover, we calculate the Fisher information given by δ_E [10] which represents the maximum possible information available via MM reconstruction procedures. We find that I_{δ_E} is 3 times higher ($150 I_{\delta_N}$) than MM reconstruction. This gives motivation to continue to develop and optimize our reconstruction algorithms to achieve this theoretical target.

In some previous works, the cross correlation r^2 terms are set to unity in Eq. 16, which artificially increases the information. To compare with their results, we plot this case in the right panel of Fig. 4. We see that, in this case, the information of the logarithmic density mapping is much higher than it is in the left panel. In the analysis of BAO or extracting other primordial cosmological parameters, we should take into account the correlation term r^2 to propagate final fields back to initial conditions [5]. This also answers the question of section 4 (*Information about what?*) of Harnois-Déraps et al. [5].

Another way to quantify the nonlinear scale of δ_α is via the information plateau's linear equivalent scale, k_{LEq}, satisfying

$$I_{\delta_L}(k_{\mathrm{LEq}}) = I_{\delta_\alpha}(k \to \infty). \qquad (20)$$

[I don't like the subscript LEq, very strange.] In the left panel of Fig. 4, we can see that k_{LEq} is just the scale on which the horizontal dashed line crosses I_{δ_L} curve. Practically, we take $I_{\delta_\alpha}(k \to \infty)$ to be I ($k = 2.7\ h/\mathrm{Mpc}$) where r goes down to zero already. We find that for δ_N, $k_{\mathrm{LEq}} \simeq 0.15\ h/\mathrm{Mpc}$. The MM reconstruction increases k_{LEq} to $0.4\ h/\mathrm{Mpc}$, whereas the logarithmic density mapping method only increases it to $0.19\ h/\mathrm{Mpc}$.

V. CONCLUSION

The MM reconstruction method successfully recovers the lost linear information on mildly nonlinear scales and increases the saturated information from $I \simeq 2.5 \times 10^{-5}/(\mathrm{Mpc}/h)^3$ to at least $I \simeq 1.3 \times 10^{-3}/(\mathrm{Mpc}/h)^3$. The result is better than previous methods, e.g. [2–4, 21].

(i) 50 or 150 times more information is quoted as the $k \to \infty$ case, which is in anyways unachievable. Within our scales of interest (BAO) $I_{\delta_R}(< k_{\mathrm{BAO}}) \simeq I_{\delta_E}(< k_{\mathrm{BAO}})$. Thus, further optimizing the code does not improve the BAO accuracy. Furthermore, the bottleneck is the number density Poisson noise and bias from surveys. I hope Yu Yu give more comments here.
(ii) Even assume we optimized (i) and regardless of BAO, 150/5=3 times more $I(< k)$ means lowering the error bar by factor of 1.7; whereas 50/1=50 times more information means lowering the error bar by 7. The latter is of much more importance.
(iii) if you compare (ii) between MM and standard reconstruction (e.g. reconstruction part in [5]), then you can quantify how much better MM is better than standard reconstruction in terms of Fisher information.
(iv) The next step/work by Xin et al. will give a direct answer to (iii) in terms of the accuracy of BAO dilation scale.

[1] D. H. Weinberg, MNRAS **254**, 315 (1992).
[2] M. C. Neyrinck, I. Szapudi, and A. S. Szalay, ApJ **698**, L90 (2009), 0903.4693.
[3] T.-J. Zhang, H.-R. Yu, J. Harnois-Déraps, I. MacDonald,

and U.-L. Pen, ApJ **728**, 35 (2011), 1008.3506.
[4] H.-R. Yu, J. Harnois-Déraps, T.-J. Zhang, and U.-L. Pen, MNRAS **421**, 832 (2012), 1012.0444.
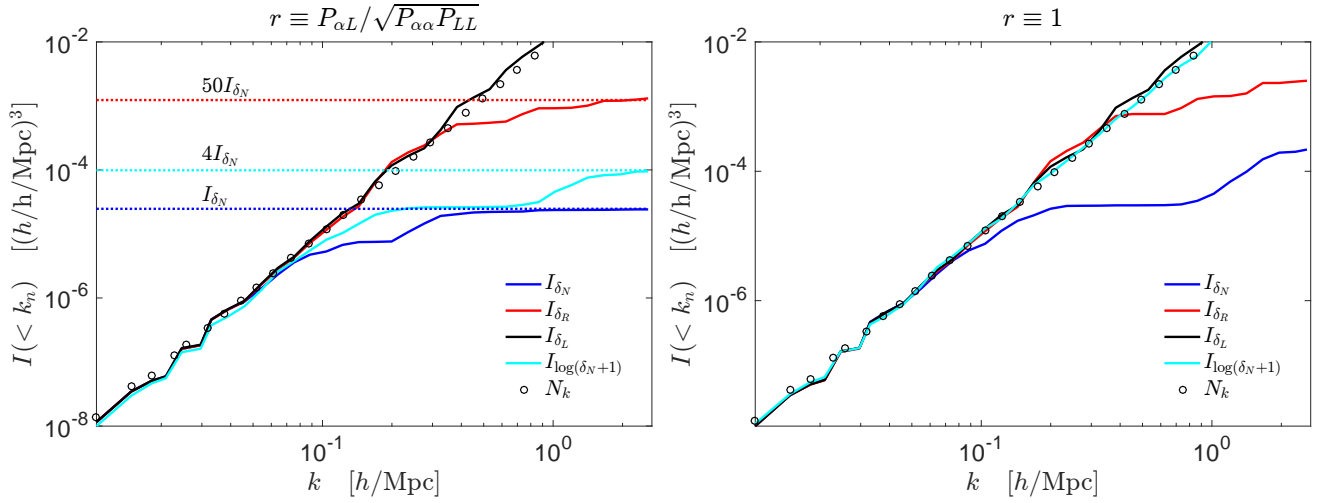[5] J. Harnois-Déraps, H.-R. Yu, T.-J. Zhang, and U.-L. Pen,

FIG. 4: *Left.* The Fisher information (solid lines) per unit volume as a function of wave number. The blue, red, black curves correspond the power spectra of δ_N, δ_R and δ_L respectively, and the cyan curve corresponds to the logarithmic density mapping. The circles are the cumulative number of k modes. Dotted horizontal lines indicate the value of the Fisher information at $k \simeq 2.7$ $h/$Mpc. *Right.* Same as the left panel except with $r \equiv 1$. The black, blue and cyan lines match the results in [2, 7].

    MNRAS **436**, 759 (2013), 1205.4989.

[6] D. J. Eisenstein, H.-J. Seo, E. Sirko, and D. N. Spergel, ApJ **664**, 675 (2007), astro-ph/0604362.

[7] C. D. Rimes and A. J. S. Hamilton, MNRAS **360**, L82 (2005), astro-ph/0502081.

[8] D. J. Eisenstein, H.-J. Seo, E. Sirko, and D. N. Spergel, ApJ **664**, 675 (2007), astro-ph/0604362.

[9] Y. B. Zel'dovich, A&A **5**, 84 (1970).

[10] H.-R. Yu, U.-L. Pen, and H.-M. Zhu, ArXiv e-prints (2016), 1610.07112.

[11] H.-M. Zhu, U.-L. Pen, and X. Chen, ArXiv e-prints (2016), 1609.07041.

[12] U.-L. Pen, ApJS **100**, 269 (1995).

[13] U.-L. Pen, ApJS **115**, 19 (1998), astro-ph/9704258.

[14] H.-M. Zhu, Y. Yu, U.-L. Pen, X. Chen, and H.-R. Yu (2016), 1611.09638.

[15] J. Harnois-Déraps, U.-L. Pen, I. T. Iliev, H. Merz, J. D. Emberson, and V. Desjacques, MNRAS **436**, 540 (2013), 1208.5098.

[16] A. Lewis, A. Challinor, and A. Lasenby, ApJ **538**, 473 (2000), astro-ph/9911177.

[17] R. van de Weygaert, A&A **283**, 361 (1994).

[18] M. Tegmark, A. N. Taylor, and A. F. Heavens, ApJ **480**, 22 (1997), astro-ph/9603021.

[19] K. Akitsu, M. Takada, and Y. Li, ArXiv e-prints (2016), 1611.04723.

[20] R. Takahashi, N. Yoshida, M. Takada, T. Matsubara, N. Sugiyama, I. Kayo, A. J. Nishizawa, T. Nishimichi, S. Saito, and A. Taruya, ApJ **700**, 479 (2009), 0902.0371.

[21] M. C. Neyrinck, I. Szapudi, and C. D. Rimes, MNRAS **370**, L66 (2006), astro-ph/0604282.